SIMULATION-BASED DESIGN OF SOLAR PHOTOVOLTAIC ENERGY GENERATION SYSTEM FOR MANUFACTURING SUPPORT

by

Milana S. MEDOJEVIĆ[a], Milovan M. MEDOJEVIĆ[a*], and Pablo DIAZ VILLAR[b]

[a] Faculty of Technical Sciences, University of Novi Sad, Novi Sad, Serbia
[b] Escuela Politecnica Superior, Universidad de Alcala, Alcala de Henares, Madrid, Spain

Original scientific paper
https://doi.org/10.2298/TSCI190719161M

Having in mind that energy is being regarded as indispensable to the socio-economic progress of developing and developed nations, where the main objective implies replacement and reduction of a major portion of the fossil fuels utilization, implementation of renewable energy technologies where natural phenomena are transformed into beneficial types of energy are becoming more and more appreciated and needed. Among renewable energy resources we know today, solar energy is the most beneficial, relatively limitless, effective, and dependable. Having this in mind, the aim of this paper is primarily to help key decision-makers understand the process when considering integration of solar energy to meet their own manufacturing energy needs, or how it is called today, to become "prosumers". Given the aforementioned, this paper provides an overview of detailed simulation methodology for photovoltaic system sizing and design for metal-forming manufacturing system energy needs. The simulation is based on National Renewable Energy Laboratory photovoltaic performance model which combines module and inverter sub-models with supplementary code to calculate a photovoltaic power system's hourly AC output is given a weather file and data describing the physical characteristics of the module, inverter, and array. Furthermore, the characteristic losses are calculated and presented for a fixed array photovoltaic system and illustratively given in the form of a Sankey diagram. A variety of graphical data representations are available while the most important ones are given in the study. Lastly, future research topics were filtered and briefly summarized.

Key words: *solar photovoltaic, manufacturing system, energy, simulation, losses, system dynamics*

Introduction

It is generally known that most modern societies depend on fossil fuels as sources of energy for development and growth. On the other hand, switching to RES, such as photovoltaic (PV) systems, is necessary for sustainable development in the future. Currently, it is much more efficient to use fossil fuels to develop PV power plants than to combust the same amount of fossil fuels in conventional thermal power plants for a variety of growing energy needs. Thus, the sooner PV systems are developed, the sooner society will reduce its reliance on fossil fuels [1]. Thanks to the massive price declines achieved in recent years and continued today [2], solar power is now broadly recognized as a cost-competitive, reliable and sustainable energy source. Based on its technical characteristics, PV can and should be consid-

* Corresponding author, e-mail: medojevicmilovan@gmail.com

ered as a low-risk investment for the financial community today. Its market uptake is strongly dependent on a stable and forward-looking regulatory framework that allows the realization of the full competitive potential of solar power [3]. Having in mind that it is the industry that drives the economy of modern societies, greening the economy drivers secures a self-sustainable future. This is especially important since energy costs have been rising over the last decades, and manufacturers start to consider energy as a valuable resource instead of an overhead cost item. All forms of energy supply and consumption can cause undesirable emissions (*e.g.* CO_2 equivalent) which contribute to environmental problems [4] while binding to emission reduction targets, such as the Kyoto Protocol add extra pressure to the manufacturing sector [5]. Additionally, the growing demand of consumers for eco-products was spotted [6]. Therefore, more and more manufacturers take action towards increasing their energy efficiency to remain competitive but also considering switching from conventional energy generation systems to renewable ones to contribute to pollution prevention and reduction. After all, systematically addressing energy generation, consumption, and related costs is a major challenge nowadays among leading manufacturers [7].

In today's market, an apparent extent of solar databases and simulation-based programs could be found available for analyzing PV systems. Logically, solar resource information is needed in all phases of a PV system development, where reliable data are required for system siting, design, operation, financing, *etc.* In most cases, monthly averages, probability statistics of typical meteorological years (TMY) are more than enough, especially considering the manufacturing industry and policymakers defining support programs [8]. However, additional solar databases such as NASA – Surface meteorology and solar energy database, RETScreen solar database, PVGIS solar database, HelioClim-1, Metenorm, European solar radiation atlas, SoDa service, Solar and wind energy resource assessment (SWERA), *etc.*, may provide additional data depending on the calculation or simulation needs and purpose. Likewise, available PV software simulators are designed with different aims in mind and have various limitations for solving certain problems, where the desirable features of the software for manufacturing simulation depend on the purpose of their use. Nowadays, software for simulating PV systems could be diversified into 12 major types [9-11]. This implies an unambiguous inference that as more PV systems are installed, the increase in demand for software that can be used for design, analysis, and troubleshooting will be triggered.

Given the aforementioned, this paper is aimed primarily to help key decision-makers in the industry to understand the process while considering the integration of solar energy to become prosumers. The scientific contribution of this manuscript is reflected in a holistic methodological approach that aims to provide a clear and unambiguous account of a series of steps necessary to consider for the integration of PV systems into the power distribution system at the manufacturing system level.

Moreover, special attention is paid to the losses occurring on an annual basis due to the energy transformations within applied technology and natural climatic characteristics specific to the site of system implementation. For research purposes, this has been done on an example of a metal-forming manufacturing system whose characteristics are given hereinafter.

A detailed National Renewable Energy Laboratory (NREL) System Advisor Model (SAM) simulation methodology for PV system design and sizing has been proposed accompanied by the obtained results. The SAM is a techno-economic computer model designed to facilitate decision making for people involved in the renewable energy industry targeting project managers and engineers, financial and policy analysts, technology developers, as well as researchers. Moreover, SAM is an open-source software package, meaning that its source code is available to the public. This implies that researchers can study the code to understand the model algorithms, while software programmers can contribute their models and enhancements to it. Having this in mind, a specific set of tools is available to create applications that interact with the SAM simulation core and integrate its models to existing software solutions already present in manufacturing facilities.

The transition to sustainable electricity supply based on renewable resources is a crucial global project of utmost importance in responding to climate change [12]. The greatest progress of PV system deployment is spotted within establishing large scale electricity generation plants worldwide [13]. However, although solar energy is a readily available source of energy, and although being recognized as non-polluting and relatively maintenance-free [14], its integration into manufacturing energy supply systems remains in infancy.

On the other hand, it became more than evident that the era of Industry 4.0 is upon us, where manufacturing companies are facing strong demand to increase their productivity by realizing smart factories and smart manufacturing, whereby when they embark on efforts to introduce this Industry 4.0 concept, they mostly focus on the core parameters of production efficiency, quality, and cost, which is obviously what drives revenue [7]. Notwithstanding it is of vital importance to establish a solid industrial ecosystem that contributes to a high percentage of national GDP, among many factors that need to be optimized to stay competitive and environmentally friendly, one is sustainable energy generation and supply which is still easily forgotten in most companies.

From this perspective, it is all about being environmentally aware and efficient in the way the energy within manufacturing system is being supplied and used, to reduce consumption where necessary, reduce harmful emissions and provide adequate information to relevant personnel across the organization to bring the same value with less sustainably-generated energy.

Simulation methodology

As previously indicated, simulation is based on NREL SAM PV performance model which combines specified modules and inverters with supplementary code to calculate a PV system's hourly AC output for a given weather file and data, describing the physical characteristics of the module, inverter, and array [15]. The model calculates the system's AC electrical output over one year as an array of 8760 hourly AC power values. It reads hourly solar resource and temperature data from a weather file, describing the resource at the system's location for the year, and uses them with inputs describing the system's design in equations to calculate module and inverter conversion efficiencies as well as related energy losses. The module and inverter model calculate solar energy to DC electricity and DC to AC electricity conversion efficiencies, respectively, and account for losses associated with each component. For the sake of simplicity, simulation procedure is described through eight main steps (S1-S8), while associated sub-steps related to S1 and S6 are indicated with letters (A-E). The given model performs the following calculations for each time step in one year as follows:

– (S1) For each array (or up to four sub-arrays):
  A. Calculate sun angles from date, time, and geographic position data from the weather file.
  B. Calculate the nominal beam and diffuse irradiance incident on the plane of array (POA) irradiance. This depends on the solar irradiance data in the weather file, Sun angle calculations, user-specified sub-array parameters such as tracking and orientation parameters, as well as backtracking option for one-axis trackers.

C. Apply the user-specified beam and diffuse nearby-object shading losses to the nominal beam and diffuse POA irradiance.
D. For fixed sub arrays and subarrays with one-axis tracking and self-shading enabled, calculate and apply the self-shading loss factors to the nominal beam and diffuse POA irradiance.
E. Apply user-specified monthly soiling factors to calculate the effective POA irradiance on the sub-array.

– (S2) For sub-arrays with no tracking (fixed) and self-shading enabled, calculate the reduced diffuse POA irradiance and self-shading DC loss.
– (S3) Determine the sub-array string voltage calculation method.
– (S4) For each of up to four sub-arrays, run the module model with the effective beam and diffuse POA irradiance and module parameters as input to calculate the DC output power, module efficiency, DC voltage, and cell temperature of a single module in the sub-array.
– (S5) Calculate the sub-array string voltage using the method determined in (S3).
– (S6) For each subarray, calculate the array DC power:
  A. Apply the fixed self-shading DC loss to the module DC power if it applies.
  B. Calculate the sub-array gross DC power by multiplying the module DC power by the number of modules in the sub-array.
  C. Calculate sub-array DC power by multiplying the gross sub-array power by the DC loss.
  D. Calculate the sub-array string voltage by multiplying the module voltage by the number of modules per string.
  E. Calculate the array DC power by adding up the sub-array values.
– (S7) Run the inverter model to calculate the gross AC power and inverter conversion efficiency.
– (S8) Calculate the AC power by applying the AC loss to the gross AC power.

Sun position model

Sun position algorithm is based on the Michalsky method [16], which algorithm has been modified to calculate Sun azimuth angles for locations south of the equator using the Iqbal [17], approach adjusted by O'Brien [18]. The first step in the sun position algorithm is to determine the effective time of the current time step in the weather file [15]. The next step considers the determination of the altitude, α, declination, δ, and zenith angle, Z. The SAM also calculates the sun azimuth angle, γ, by using the Iqbal approach. Furthermore, the equations describing the Sunrise and Sunset Hours model were summarized by Gilman [15], followed by a sunup flag* indicating whether the Sun is above or below the horizon in the current time step. Lastly, to calculate POA irradiance it is necessary to determine extra-terrestrial radiation, H, beforehand. For these purposes, the extra-terrestrial radiation model equation is adopted from Duffie and Beckman [19].

Surface angles model

Here, each sub-array in the system is considered as a flat surface with one tilt angle, β_s, and one azimuth angle, γ_s, that define the surface orientation. In this paper, a simulation was carried out for a fixed PV system, while the surface angle equations are based on standard

* The sunup flag only reports the sunrise and sunset hour for hourly data and it is used by PV model to determine whether to calculate the cell temperature in the current time step.

geometric relationships defined by the surface orientation and previously defined sun angles. Surface angles of each sub-array are calculated for each time step of the simulation, while variables used for the surface angles determination were adopted from Dunlap [20]. After defining the surface angles it is possible to determine the angle of incidence (AOI). The AOI is a function of the Sun azimuth angle, γ, Sun zenith angle, Z, surface azimuth angle, γ_s, and the surface tilt angle, β_s.

The POA irradiance model

The POA irradiance is being calculated for the sunrise, sun-up, and sunset time steps. The incident angle algorithm calculates the beam and diffuse irradiance incident on the PV sub-array surface for a given Sun position, latitude, and surface orientation. For each time step in the simulation, the POA irradiance algorithm performing steps is given in fig. 1.

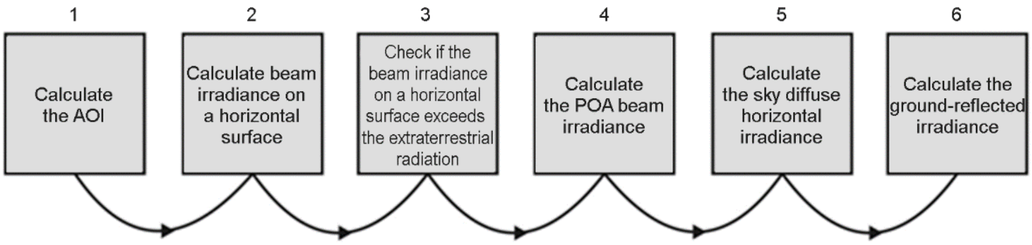

Figure 1. The POA irradiance algorithm steps

In this case, POA irradiance data from the weather file were applied for simulation purposes. In cases where these data are not available, they could be calculated according to the Freeman *et al.* [21] model. Subsequently, SAM compares the beam irradiance on a horizontal surface, I_{bh}, to the extraterrestrial radiation, H, where if $I_{bh} > H$, the software generates an error flag that causes the calculations to stop. Determination of POA sky diffuse irradiance, I_d, is performed based on the Perez model. The Perez model uses a more complex computational method than the other two available methods and involves some empirical relationships and calibration. It accounts for both isotropic and circumsolar diffuse radiation, as well as horizon brightening. Perez sky diffuse irradiance model was adopted from PV Watts [22] and described by Perez *et al.* [23, 24], while the updated general description of the model could be found in the more recent study [25]. The Perez transposition model has the smallest root mean squared difference (RMSD) at all locations, indicating it may be the best model choice when measured DHI is available.

Lastly, The POA ground-reflected irradiance, or the solar energy that reaches the array surface after reflecting from the ground represents the function of the beam normal irradiance, Sun zenith angle, sky diffuse irradiance, and ground reflectance (albedo) defined by Liu and Jordan [26]. Bearing in mind that the ground reflects light diffusely, the ground-reflected irradiance is considered as diffuse irradiance.

Effective POA irradiance model

The effective POA irradiance is the solar irradiance incident on the array less any due to external shading, self-shading, and soiling. On the other hand, a term nominal POA irradiance is introduced to represent the sum of the beam POA irradiance, sky diffuse POA irradiance, and ground-reflected POA irradiance. External shading stands for situations when objects near the PV array (such as trees, buildings, roof protrusions, and parapets) cast shadows on the array and thus reduce both the beam and sky diffuse POA irradiance, which in turn reduces the array's DC electrical output. The shading loss inputs are expressed as percentages, which indicates that each percentage should be converted to a factor using the equation introduced by Gilman *et al.* [15]. On contrary to previously mentioned, self-shading occurs when PV modules are arranged in parallel rows, and modules in one row cause a shadow on modules in a neighboring row. In this case, a self-shading model for fixed subarrays was applied to determine the minimum distance between strings to avoid it as much as possible. The equations and algorithms used to calculate self-shading losses are described in [27, 28].

The PV module models

The module model selected for the simulation purpose in this research was the CEC module model based on the implementation of the single-diode equivalent circuit model of a PV module described by De Soto [29, 30]. Additionally, NOCT cell temperature model was applied to calculate the cell temperature, T_c, while the detailed calculation procedure was provided by Gilman *et al.* [15].

However, both module and temperature models are based on the following assumptions. Foremost, all modules in the system operate at their maximum power point, except for the sub-array mismatch and inverter operating voltage limit losses described hereinafter. Subsequently, the sub-array maximum power point is determined by the maximum power point of a single module and the number of modules per string. All sub-arrays in the system have the same number of modules per string and therefore operate at the same voltage. Lastly, it is considered that all modules in each sub-array operate uniformly, which excludes module mismatch losses from further calculations. However, practical implementation proved the opposite and the rule of thumb suggests considering these losses in setups with long strings without DC optimizers or micro-inverters.

Array DC output model

In this section, a brief description of the array DC output model is provided. In the beginning, it is necessary to calculate each sub array's DC output by multiplying a single module's DC output by the number of modules in the array. To achieve this, it is necessary to calculate the array's operating voltage in each time step to determine the inverter's input voltage, assuming that each module operates at its maximum power point. Having in mind the availability of data regarding the open-circuit voltage, V_{oc}, and short circuit current, I_{sc}, of each subarray, the necessary calculations are performed within the selected PV module model. Moreover, the power output of each sub-array represents the product of the number of modules in the subarray and the DC loss factors associated with the sub-array. The most common losses here are self-shading DC loss, DC electrical losses, DC snow-coverage losses, and mismatch losses, which detailed determination procedure is provided by Gilman *et al.* [15], Marion [31] and Ryberg [32], respectively.

Inverter AC output model

To determine the inverter AC output Sandia inverter model was used. This model stands for an empirical model that uses manufacturer specifications with four empirically derived coefficients C_0, C_1, C_2, and C_3 described by King *et al.* [33]. The inverter model calculates the inverter's DC to AC power conversion efficiency at rated and part-load operating power. However, this model does not explicitly account for the effect of temperature on inverter performance or for the impact on inverter performance of power factor control or grid outages. Here two kinds of inverter losses (clipping) should be considered. First one is related to MPPT clipping, a reduction in the inverter DC input power when the input voltage (DC string voltage) falls outside of the operating range defined by the inverter's minimum and maximum MPPT DC voltage ratings, while the second one considers power clipping, a reduction in the inverter output AC power, caused by inverter saturation when the inverter power exceeds its nameplate rating.

Degradation modeling

Having in mind that PV modules lose their performances over time, the reduction in the array's output due to degradation of the module cover and other causes should be considered. This applies to both the AC and the DC part of the system. The SAM suggests an integration of degradation value as a percentage on an annual basis, where the general rule of thumb states that PV panels degrade between 0.5-1% each year.

System AC output model

The system AC output is the electricity generated by the PV system and may be delivered to a manufacturing facility in this case. Before the determination of useful power generated by the system, two types of losses should be taken into account. These are electrical losses on the AC side of the system given as a single AC loss percentage, curtailment and availability losses used to account for operating losses imposed on the system by factors other than the solar resource and system's design, such as forced, scheduled, and unplanned outages, or other factors that reduce the system's AC power output. Finally, the power generated by the system result variable as electricity generated by the PV system after all losses and adjustments, and represents the electricity delivered to the observed manufacturing system.

System sizing and design

In this section, relevant information regarding the manufacturing facility in terms of electrical load, system sizing and design are provided. Here, to properly define system size weather conditions at the observed location, selected PV modules and inverter types, sun tracking and related system losses were considered.

Manufacturing system specification

For the analysis purposes, a metal forming manufacturing system was selected. The observed system is a custom-based machining facility specialized in the field of automotive and aviation industry with a focus on machine-made parts, details, components, assemblies, and fixtures in quantities of single-piece prototypes to a large volume production machining. The process is performed on CNC machining centers, milling machines, and lathes. Factory's machine park consists of the machines listed as follows: Schmid VMC-800P, Schmid VMC-500P, Leadwell MCV-600XL, Takang TNC 05, Kia KT 15, Haas SL-20 THE, Haas ST-20 Y, Haas ST-20 HE, and Kasto SBA-260AU. These are followed by small manual lathe, milling, and cutting machines, table grinders, measuring devices (Zoller H-320 and U Soft C-400), Alup Solo 18 screw compressor and Alup ADQ air dryer. The aforementioned equipment is considered as significant energy users and represents the main variable in the process of energy-related behavior profiling. Also, overall energy consumption considers factory lighting and ICT systems. The factory layout is shown in fig. 2.

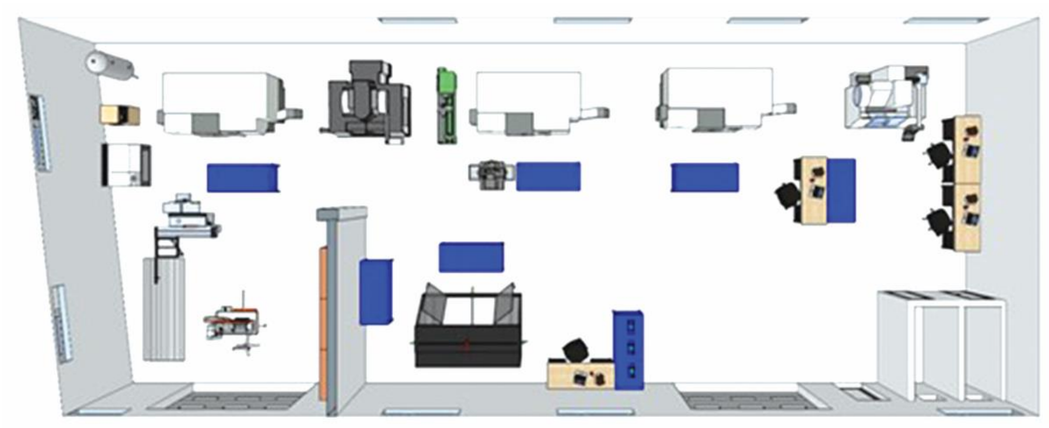

Figure 2. Factory layout with machine positions

In addition, annual electricity consumption on a monthly basis is given in tab. 1 and represents the manufacturing energy load which could be partially provided by a PV system.

Table 1. Overall manufacturing system annual electricity consumption on a monthly basis

Month	Jan.	Feb.	Mar.	Apr.	May	June	July	Aug.	Sept.	Oct.	Nov.	Dec.
EC*	4460	4578	4022	4234	3567	4121	3967	4429	3876	4785	4013	4238

* EC – energy consumption [kWh]

Manufacturing activities are scheduled in two shifts, while the working hours are in the interval from 6 to 22 hours. This information is important since in the design of PV system, in this case, no batteries are considered. This means that in the lack-of-energy situations electricity is withdrawn from the electricity grid while the surplus is distributed to the grid.

System sizing

As previously mentioned, system sizing consists of several steps starting from defining weather conditions at the observed location which are briefly summarized in tab. 2.

Table 2. Weather conditions at observed location

Station ID	131681	Global horizontal	3.96 kWh/m^2 per day
Data source	ISD-TMYx	Direct normal (beam)	3.31 kWh/m^2 per day
Elevation	87 m	Diffuse horizontal	1.91 kWh/m^2 per day
Latitude	45.25 °N	Average temperature	10.5 °C
Longitude	19.883 °E	Average wind speed	3.0 m/s
Time zone	GMT +1	Maximum snow depth	28 cm
		Annual albedo	–999

Subsequently, the selection of PV modules and inverter was performed. Table 3 summarizes relevant module characteristics at referent conditions and associated temperature coefficients, while in fig. 3(a) I-V curve diagram was given.

Table 3. Module characteristics at referent conditions and associated temperature coefficients

Module characteristics at ref. conditions		Temperature coefficients		Physical characteristics	
Nominal efficiency	20.5521%			Material	Mono-c-Si
Maximum power, P_{mp}	335.2 Wdc	–0.310% per °C	–1.039 W per °C	Module width	1 m
Max power voltage, V_{mp}	57.3 Vdc			Module height	1.63 m
Max power current, I_{mp}	5.8 Adc			Module Assrea	1.63 m^2
Open circuit voltage, V_{oc}	67.9 Vdc	–0.25% per °C	–0.17 V per °C	No. of cells	96
Short circuit current, I_{sc}	6.2 Adc	0.04% per °C	0.002 A per °C		

In terms of a mounting standoff, modules are building integrated, placed on the rooftop of 5 m high one-story facility building. Also, the model assumes a reference band-gap voltage $E_{g,ref}$ = 1.121 eV, and temperature coefficient for band-gap of –0.0002677 eV/K, while the additional parameters relevant for calculation are given in tab. 4.

Table 4. Module-related additional calculation parameters

Module NOCT temperature rating, T_{noct}	46.4 °C
Reference ideality factor, A_{ref}	2.42033 V
Reference light current, $I_{L,ref}$	6.23681 A
Reference diode saturation current, $I_{o,ref}$	3.98831e^{-12} A
Series resistance, R_s	0.499389 Ω
Reference shunt resistance, $R_{sh,ref}$	457.185 Ω

Furthermore, the relevant characteristics of a selected inverter are listed in tab. 5, while the efficiency curve is given in fig. 3(b).

Table 5. Relevant characteristics of the selected inverter

Inverter characteristics		Sandia coefficients	
Number of MPPT inputs	1	C_0	–3.08e^{-06} 1/Wac
CEC weighted efficiency	97.053%	C_1	–4.8^{e-05} 1/Vdc
European weighted efficiency	96.676%	C_2	–0.000124 1/Vdc
Maximal AC power	3850 Wac	C_3	–0.001632 1/Vdc
Maximal DC power	3964.41 Wdc		
Power consumption during operation	17.8856 Wdc		
Power consumption at night	1.155 Wac		
Nominal AC voltage	240 Vac		
Maximal DC voltage	480 Vdc		
Maximal DC current	9.91101 Adc		
Minimal MPPT DC voltage	100 Vdc		
Nominal DC voltage	400 Vdc		
Maximal MPPT DC voltage	480 Vdc		

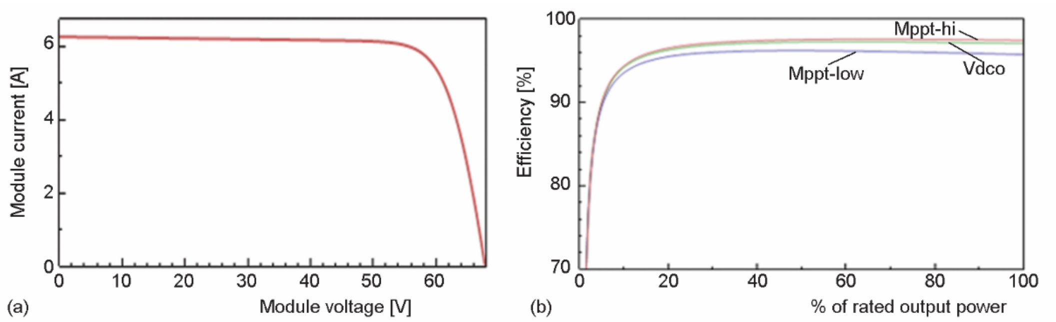

Figure 3. The PV module I-V curve diagram (a) and inverter efficiency curve (b)

After the consideration of the described weather file and selection of PV module and inverter type, it is possible to begin with system design. The available rooftop area amounts 276 m^2, which represents the limiting factor for PV array set-up, while additional limitation is related to modules self-shading. Having this in mind, the system sizing summary is given in tab. 6.

Table 6. The PV system sizing summary

System sizing		AC sizing	
Total AC capacity	34.65 kWac	Number of inverters	9 pcs
Total inverter DC capacity	35.68 kWdc	DC to AC ratio	1.28
Nameplate DC capacity	44.247 kWdc	DC sizing	
Total number of modules	132 pcs	String Voc at ref. conditions	407.4 V
Modules per string in array	6 pcs	String Vmp at ref. conditions	343.8 V
Total number of strings	22 pcs		
Total module area	215.3 m^2		

Lastly, tab. 7 provides relevant information regarding PV system tracking and orientation, as well as subsequently determined system losses.

Table 7. The PV System tracking and orientation, and system losses

Tracking and orientation			System losses	
Tracking	No (fixed)	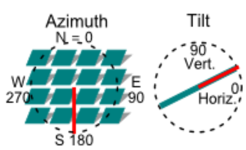	Average annual soiling	5%
Tilt	34 °		Module mismatch	2%
Azimuth	180 °		Diodes and connections	0.5%
Ground coverage ratio	0.3		DC wiring	2%
Shading	No		AC wiring	1%
Snow losses estimation	Yes		System availibility	3%
Row spacing estimate	5.55048 m		System degradation	0.5% per year
Self-shading model	Standard non-linear			

All of the aforementioned represent the necessary input for the simulation of PV energy generation to ensure sustainable energy supply to the observed manufacturing system.

Simulation results and discussion

In this section relevant simulation results in terms of potential energy generation on an annual basis, annual ambient temperature and wind speed, irradiance distribution, relevant equipment efficiencies, levelized energy losses, monthly profiles, *etc.*, are given as graphical representations with concrete and brief descriptions where necessary. Primary indicators, or general PV system metrics are given in tab. 8, while the 3-D model of the system integrated within a manufacturing facility is shown in fig. 4.

Table 8. General PV system metrics

Metric	Value
Annual energy (year 1)	57.574 kWh
Capacity factor (year 1)	14.9%
Energy yield (year 1)	1.301 kWh/kW
Performance ratio (year 1)	0.78

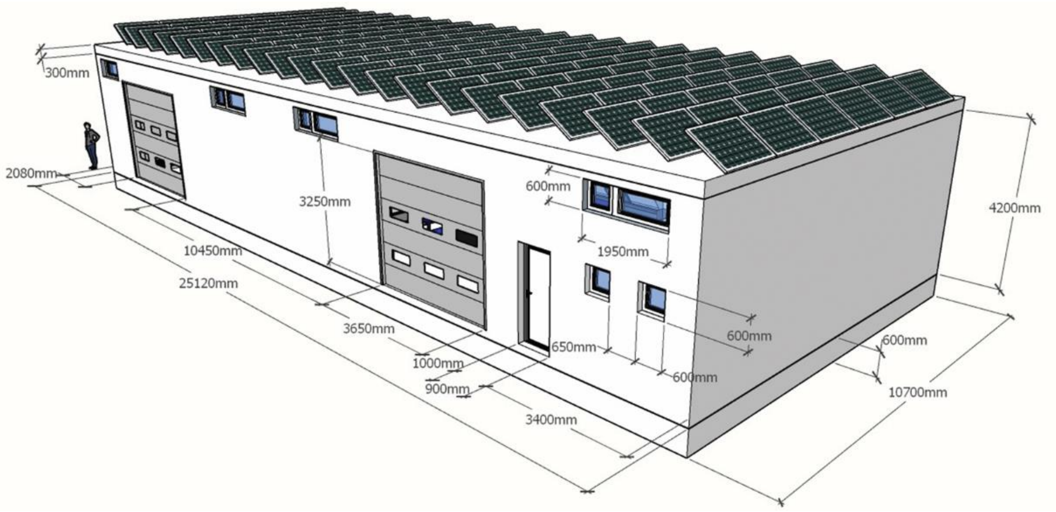

Figure 4. The 3-D model of the PV system integrated into a manufacturing facility

Besides, annual solar resource availability distribution at the observed location in terms of direct normal (DNI), diffuse horizontal (DHI), and global horizontal (GHI) irradiance is given on an hourly basis in the fig. 5. Likewise, fig. 6 shows PV system DC and AC annual energy generation, as well as electricity load from the manufacturing site monthly.

An hourly overview regarding PV system energy generation and consumption on an annual basis is given in fig 7.

To provide clear insight regarding the available Sun power and effective power load that could be generated by the designed PV system, monthly profiles were created and given in fig. 8.

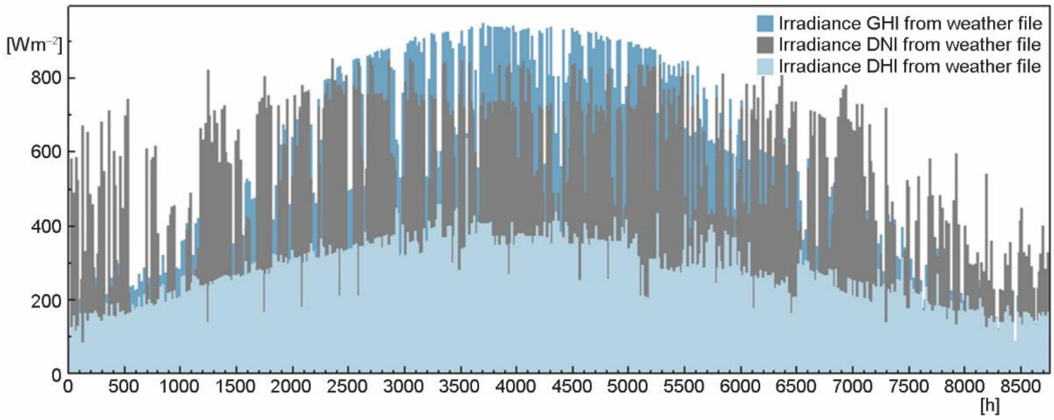

Figure 5. Annual solar resource availability distribution on an hourly basis (DNI, DHI, and GHI)

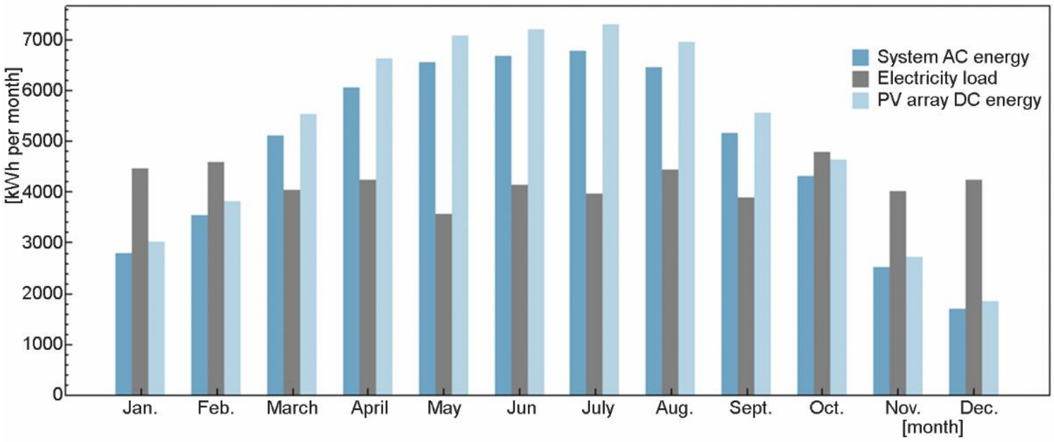

Figure 6. The PV system energy generation (AC and DC) and electricity load on a monthly basis

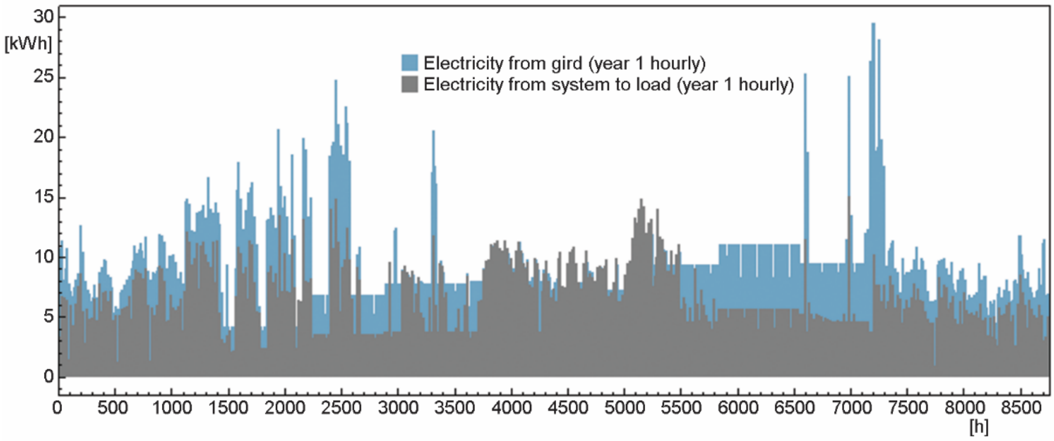

Figure 7. Hourly PV system energy generation and consumption on an annual basis

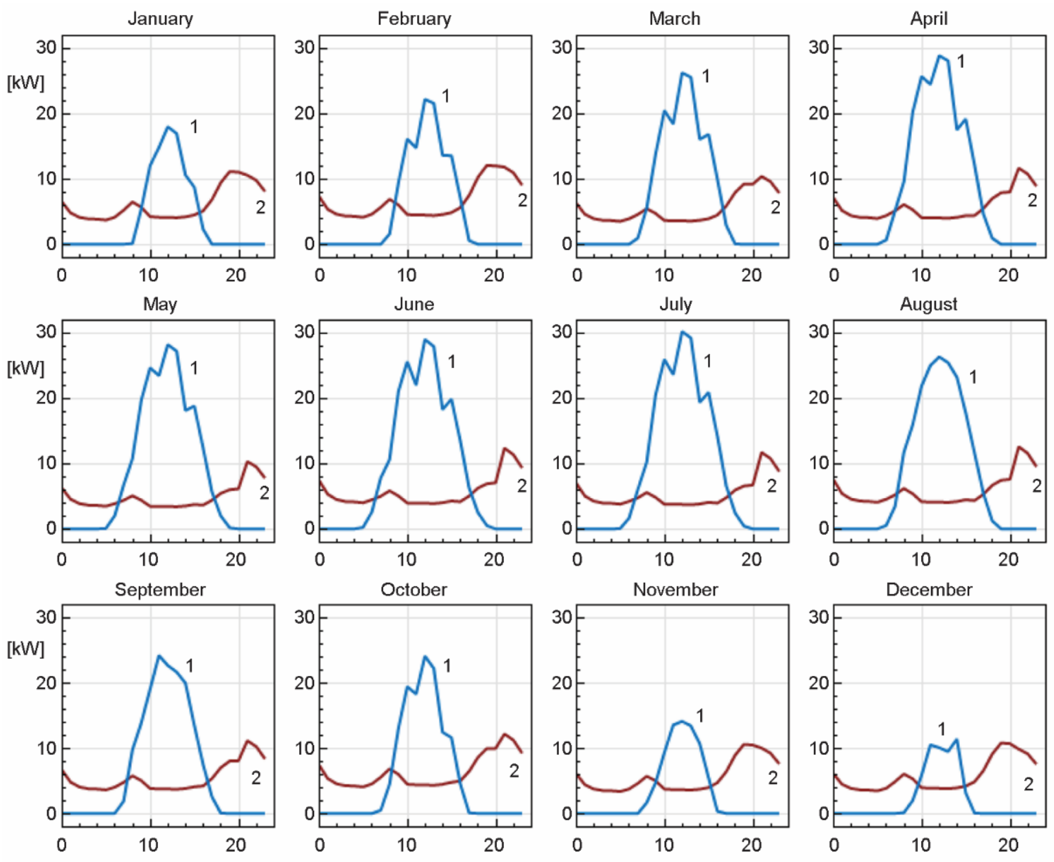

Figure 8. Monthly profiles of total available and system-generated power; *1 – lifetime hourly data: system power generated [kW] and 2 – lifetime hourly data: lifetime electricity load [kW]*

Here, monthly profiles show the average daily profile in each month of the year for the selected variables. In this case, selected variables are electricity load and system power generated. Logically, an annual profile could be calculated by averaging all of the monthly profiles. The generated profiles imply that the observed location is suitable for PV system implementation, and the significant portion of energy demand could be covered by the implementation of the proposed system. Moreover, these profiles indicate that energy storage integration could greatly contribute to the facility's self-sustainability by providing stored energy in the morning (when the irradiance is non-present and less intensive) and in the evening (when irradiance is less intensive and tends to none).

Subsequently, in the analysis of variety PV system variables, the next useful tool applied for data representation is heat maps. The heat map allows identification of how the data varies by time of day and by the time of year on the same graph. Here, the time of year is plotted on the *x*-axis, while the time of day is on the *y*-axis. This tool process only one variable at the time, while the selected ones are given in fig. 9. The heat map color is coarse rainbow, due to the fact it provides higher color resolution. The *hot-cold* color map ensures that values above zero tend toward red, while values below zero tend toward blue. Although this type of data visualization is mainly related to temperature it could be used in other cases as well. In fig. 9, the general relation between ambient temperature and cell temperature could be spotted. Data sets imply that as ambient temperature increases, the cell temperature exponentially rises. Also, module efficiency varies between 12% and 23% due to the temperature impact, where high temperatures could knockdown module efficiency as much as 50%. Simultaneously, system power generated varies between 16-35 kW.

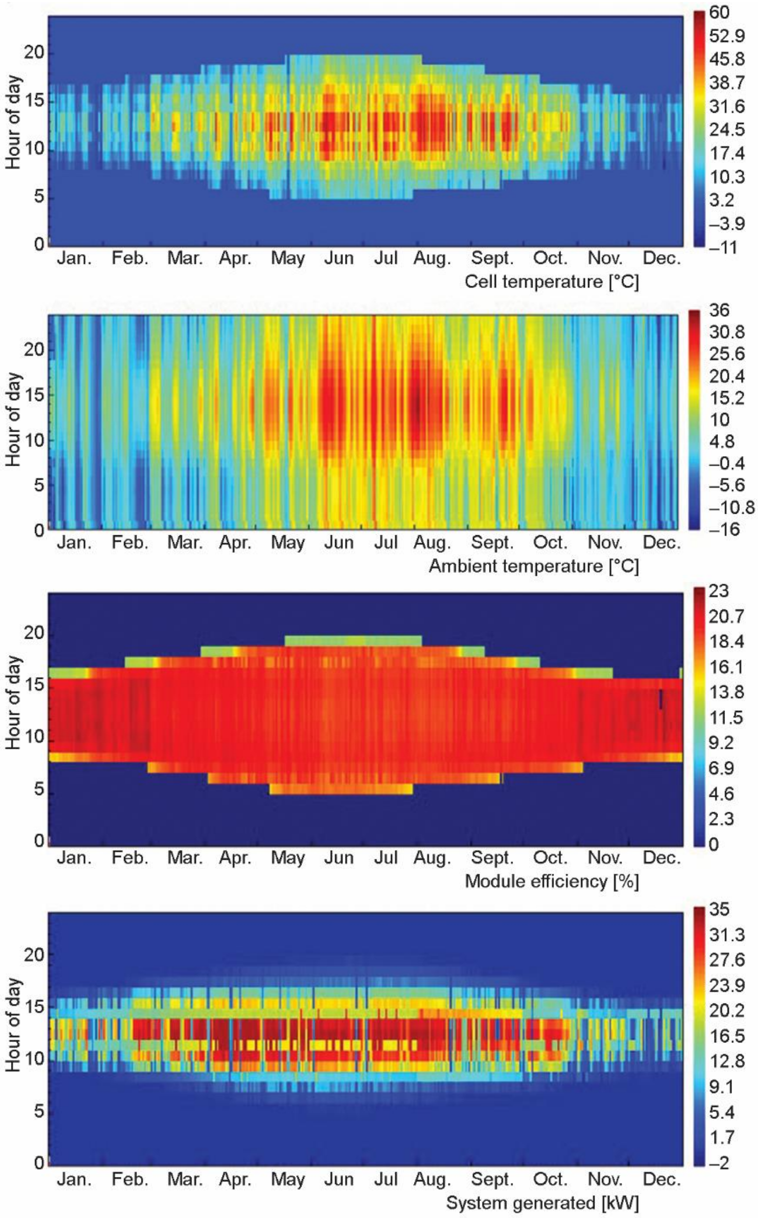

Figure 9. Selected variables representation in the form of heat map

Moreover, based on the process approach, previously mentioned losses are taken into account, associated with related process stage and illustratively given in fig. 10 in the form of a Sankey diagram, fig. 10(a). Also, fig. 10(b), provides insight on a probability density function (PDF) for a power generated by the system and system energy load in the form of data points and percentage. As previously mentioned, as well as having in mind that the module efficiency in electricity generation largely depends on surface cell temperature, fig. 10(b3) right) provides an insight regarding the correlation between these variables on a monthly ba-

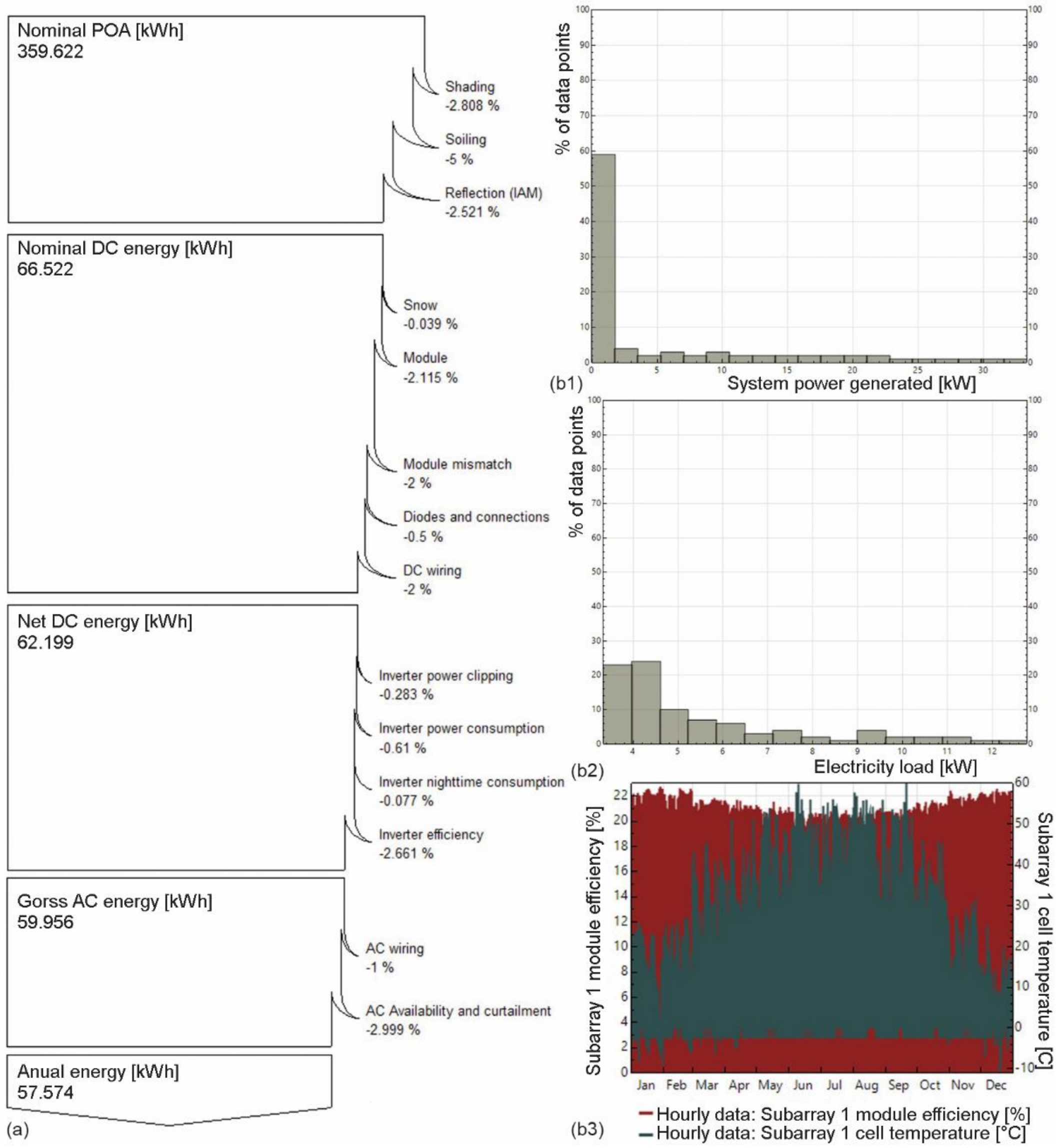

Figure 10. Typical energy losses in the observed system (a), system power generated PDF (b1), electricity load PDF (b2), and module efficiency and cell temperature correlation (b3)

sis. With the exposure of PV module to sunlight, the amount of energy from the sun converted to useful energy is about 30%, a greater percentage transforms to heat, which tends to make the temperature of the module rise. This is the main cause that leads to a reduction in electricity produced by the module as commented within fig. 9.

An increase in the temperature of the module as a result of this energy wasted as heat can damage the material used to fabricate the PV module and hence reduce the cell lifespan as well as its conversion efficiency. Finding a solution to the challenge of PV modules overheating was the subject of a large number of studies [34-43], while only some of them were referred to in this manuscript.

To be holistic it is necessary to distinct four types of loss categories within PV system implementation and operation in this specific case.

The first category (irradiance losses) covers the types of losses related to tilt and orientation, incident angle modifier, soiling, and snow coverage. The first two are obvious and well known, while the last two depend on a variety of natural/weather conditions. According to the industry standards for PV losses, it is suggested that typical soiling loss amounts to about 5% for regions with long dry seasons. If the region experiences frequent dust deposits additional 1-2% of loss could occur. Also, if the system is located near major vehicular traffic areas additional 1% should be added. Regions with year-round rain should consider increasing this type of loss by 2%, while in cases where the system will be cleaned during the summer a reduction of 0,5% should be made [44]. In the case of this manuscript, by analyzing the weather conditions and the location of the observed facility authors adopted the suggested value of 5% as soiling losses. Furthermore, snow loss is hard to estimate since it is very dependent on the micro-location. It is suggested to use monthly snow loss factors rather than annual. Snow loss can reach upward of 20% in some regions during winter months. In the case of this manuscript, snow losses were calculated (0.039%) but could be neglected for three reasons. Firstly, the calculated value is negligible. Secondly, due to climate change, it is a fact that fewer and fewer snowfalls could be noticed in the geographical region. Thirdly, the design of the solar installation, particularly the tilt of the panels, plays an important role in eliminating this loss factor effectively.

The second category (DC losses) covers the types of losses related to module nameplate rating loss, mismatch loss, light-induced degradation, wiring losses, connection losses, shade mismatch, and temperature coefficients. Module nameplate rating loss accounts for the difference in the stated power of the module from a datasheet compared with how it performs at standard test conditions (1000 W/m^2 and 25 °C). Most modern modules (as well as modules used in this manuscript) have datasheets that accurately reflect module operation at STC, so the default value for this loss is 0%. On the other hand, mismatch loss refers to losses caused by slight differences in the electrical characteristics of the installed modules, applied as a fixed percentage reduction of the system's DC power output. These losses will be higher for systems that have a wider error range on rated power. Industry research has shown mismatch values range from 0.01% up to 3%, depending on the setup of the system and the length of strings. It is suggested to use a default value of 2% based on past industry consensus in cases for most modules and systems with long strings with no DC optimizers or micro-inverters [44]. Light-induced degradation (LID) is a less-well-known phenomenon that impacts a large segment of the crystalline-silicon cell market. In short, it is the degradation that occurs in a solar cell over the first few days after the installation as a result of exposure to sunlight. This can lead to losses of 0.5-1.5%. Importantly, the LID impacts some module types but not others. In the case of this manuscript, authors carefully have chosen modules with no LID impacts, and thus eliminated this type of loss. In general LID loss can amount as 1.5% for most crystalline solar modules, 0.5% for most multi-crystalline solar modules and 0% for n-type modules [44]. Also, DC wiring losses were adopted as suggested by the National Electric Code (NEC). Here 2% loss is expected for most systems, while 1% could be achieved if using thicker wires or very short runs (very rare cases). These losses are practically inevitable because wires themselves have a small amount of internal resistance, the amount of which will be based on the gauge (thickness) of wire as well as its length. Subsequently, connection losses capture resistive losses across wiring connectors and diodes [44]. The NREL study suggests a value of 0.5% loss for these components [15]. Most solar panels contain bypass diodes, which let other modules on a string circumvent a panel that is shaded or otherwise poorly performing. These components have a small voltage drop, caused by the internal resistance of the material and imperfections in the contact surface. Moreover, in this case, external shading does not exist since there are no objects that interrupt solar irradiance. However, the self-shading losses are caused by a preceding row of PV modules and applied to all but the first row of PV modules. It is almost impossible to avoid these losses, although with careful planning they can be reduced to a minimum. In this case, the main limitation to effectively decrease this type of loss is the available rooftop area. However maximal row spacing was calculated to be 5.55 m. Normally, it is defined by the minimum solar elevation angle, γ_{min}, that can be determined at noon or any earlier hour on the shortest day of the year (on December 21 for the northern hemisphere) and given as the spacing factor at selected module's inclination angle. Temperature coefficients are however well known and clearly defined in tab. 2. However, the hotter a solar panel gets, the less efficient it becomes. The causes are grounded in physics as higher cell temperatures reduce the amount of available energy from absorbed photons as they flow through the solar panel.

The third category (AC losses) covers the types of losses related to AC wiring, inverter losses, and inverter clipping. Here, AC wiring losses may simply be defined by the distance between the inverter and the injection point and well-defined cable type. These losses can be higher than DC wiring losses if not matched specifically to the overall PV system characteristics. However, if everything is done right, AC losses account for 1% for the size of PV systems observed in this manuscript [44]. Furthermore, inverter losses are determined based on inverter efficiency which describes how well a solar inverter converts DC energy into AC energy. Most inverter spec sheets have indicated its maximum efficiency and a weighted efficiency value that is an indication of how well an inverter performs over a range of inputs. This has been straightforwardly given in tab. 4. Inverters have a variable efficiency based on what amount of capacity they are carrying, often peaking around 20% and falling slightly as the load reaches the maximum input rating. On the other hand, Inverter clipping occurs when the output from the DC solar panels at their maximum power output (or maximum power point) is greater than the amount of DC power the inverter can convert. In those cases, the inverter will operate at a non-optimal point on the I-V power curve so that it only outputs its rated maximum power. In other words, the amount of kWh production lost (or *clipped*) compared to what the system would have produced had it not been limited by the inverter rating. Inverter clipping is not a constant value across the day--clipping losses tend to occur only when the Sun is high in the sky (reducing IAM losses), and on sunny days (less shading from clouds). The systems receiving more irradiance (sunnier climates, low shade) start experiencing clipping around a 1.25 DC-to-AC ratio, while systems in cloudier climates, non-ideal orientations, or with shade do not see as much clipping until about a ratio of 1.35 [44]. In the case of this particular research, inverter clipping, as well as other types of losses and their intervals of occurance, are illustratively given in fig. 11 on hourly bases in the period of one year. The inverter clipping losses turned out to be significant in the spring period which suggests further investigation to achieve higher efficiency within the system.

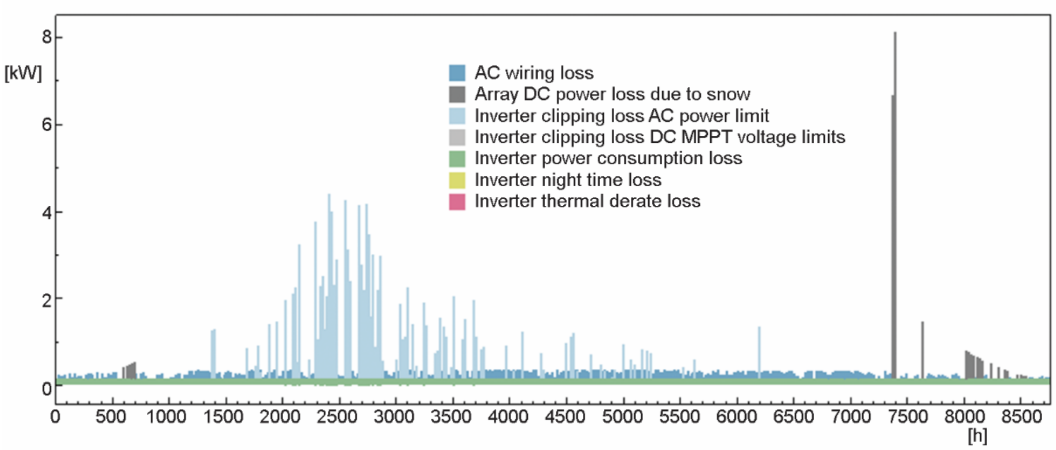

Figure 11. Identified relevant types of losses plotted on an hourly basis

Lastly, the fourth category (other losses) covers the types of losses related to system availability and system degradation (aging). System availability is a generic loss value. It is meant to capture events that knock out the system entirely, including inverter shutdowns or failures, grid outages, or other actions that disconnect the PV system and prevent it from producing electricity for the consumer. The exact timing and duration of such outages are unpredictable though, so the industry approach is to model these as a flat percentage loss spread out across the entire set of hours. Suggested values vary from 3% for most systems to as low as 0,5% if the alert system or O&M are expected to prevent downtime [44]. For security reasons, the authors of this manuscript adopted the suggested value of 3%. System degradation occurs due to the modules aging supported by the fact that the materials in solar cells lose efficiency over time. These losses need to be taken into account when analyzing the lifetime value of a project. Here suggested values vary from 0.3% per year for high-end modules, 0.5% per year for mono-crystalline to 0.6% per year for poly-crystalline modules [44].

Having in mind that the number of losses that could occur impacts the overall efficiency of the PV system.

Lastly, by conducting a comparative analysis of the energy amount on the side of demand given in tab. 1, and the amount of energy that could be supplied by proposed PV system, fig. 4, it is possible to generate a prosumer profile of observed manufacturing system provided in the fig. 12.

From fig. 12 it could be concluded that for the period from mid-October to mid-February, PV system cannot effectively supply the demand needs due to the weather conditions characteristic for this period of a year and requires energy draw from the grid. On the other hand, from the second half of February to the first half of October, PV system can cover the majority of demand-side needs and generates excess energy that could be fed into the grid according to applicable regulations and tariffs. The annual distribution of energy deficit and a surplus is given in tab. 9.

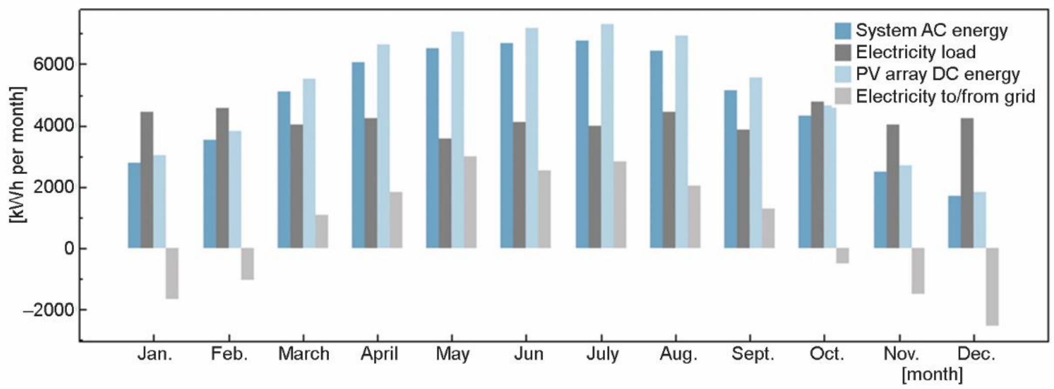

Figure 12. Generated *prosumer* profile of observed manufacturing system

Table 9. The annual distribution of energy deficit and surplus

Month	Jan.	Feb.	Mar.	Apr.	May	June	July	Aug.	Sept.	Oct.	Nov.	Dec.
A*	4460	4578	4022	4234	3567	4121	3967	4429	3876	4785	4013	4238
B*	2794	3528	5112	6063	6537	6670	6766	6449	5157	4299	2502	1696
C*	–1666	–1050	1090	1829	2970	2549	2799	2020	1281	–486	–1511	–2542

A* – electricity load; B* – PV System AC energy; C* – Electricity to/from grid [kWh per month]

However, considering monthly energy consumption data certain error occurs which means that the data shown in fig. 12 and tab. 9 must be taken into account with a certain caution. This is primarily due to the fact that the monthly consumption profiles do not include the relevant data regarding energy-related machine behavior during their operation. To obtain the most accurate estimation, it is necessary to establish a system of continuous measurement and data logging of the electrical current and voltage during machine operation. Bearing in mind that industrial systems are characterized by relatively stable voltage, measuring the electrical current at certain time intervals will result in reasonable precision regarding the energy consumption profile of the manufacturing system. The integration of these data into the simulation would provide the most accurate results. This, in turn, points to the potential focus of future research in the field.

Since energy costs are constantly increasing, manufacturers are seriously considering energy conservation while practicing energy efficiency measures and renewables integration as a cost-effective way to reduce energy consumption with two possible trajectories, first relates to devices and second to measurements and behavior. Although energy conservation measures come in many forms, they are mostly technological. However, since technology is operated by people it leads to the conclusion that the failure of the user component can block the whole mission in the energy efficiency increasing process. Consequently, it is important to increase energy efficiency by reducing energy needs and changing everyday habits in energy use, as well as strengthening end-user awareness about energy conscientiously behavior, which might further enable sustainable energy development.

Conclusions

In this paper key parameters for determining the energy performance of a conceptual, 35 kW output power, PV system was observed. From the obtained results it can be concluded that favorable conditions exist for the use of PV solar energy at observed location. The main aim of this research was to provide a holistic methodological approach to key decision-making personnel to stimulate their further engagement regarding PV systems integration into their processes. Moreover, this research revealed possible limitations for the implementation of such systems in terms of characteristic types of losses. Particularly, module efficiency could drop as to 50% due to a surface cell temperature at 60 °C or more. These efficiency drops are expected at ambient temperatures of 30 °C or more, or in other words, during late spring, summer, and early autumn periods. Another interesting finding is related to the inverter clipping losses which turned out to be significant in the spring period. This finding opens new research questions regarding further investigation to achieve higher efficiency within the system. On the other hand, the study also revealed that although being calculated, losses related to snow coverage could be neglected. Authors believe that this is mainly due to the modified weather conditions caused by climate changes.

Subsequently, the study revealed that the integration of energy storage could significantly improve the ratio of energy use from PV sources. Authors believe that if well designed, energy storage could significantly eliminate the need from energy draw from the grid. However, a detailed analysis should be carried out which indicates a rise of a new research question.

The simulation-based analysis resulted in forecasted annual energy production of 57.6 MWh with a capacity factor of 14.9%. Characteristic energy yield was calculated to be 1301 kWh/kW indicating the performance ratio amounts 0.78. Here, the temperature dependence of characteristics of PV panel is the main cause of lower performance ratio during the summer compared to the winter, which suggests consideration of enhancing the performance of PV panels by fluidic cooling where hybrid versions of panels are the most common ones in the application. Moreover, for the period from mid-October to mid-February, PV system cannot effectively supply the demand needs of the observed manufacturing system due to the weather conditions characteristic for this period of a year. On the other hand, from the second half of February to the first half of October, PV system can cover the majority of demand-side needs and generates excess energy that could be fed into electricity grid according to applicable regulations and tariffs. However, considering energy consumption data monthly, a certain error occurs which means that these data must be taken into account with a certain caution. This is primarily due to the fact that the monthly consumption profiles do not include the relevant data regarding energy-related machine behavior during their operation. To obtain the most accurate estimation, it is necessary to establish a system of continuous measurement and data logging of the electrical current during machine operation which points out the potential focus of future research in the field.

Lastly, authors are pointing out to the fact that the exponential function of technological development became peaking steep with strong pressure to eliminate boundaries between production and management, providing that ERP, MES, and other critical systems are integrated to realize the growth opportunities that this new age of intelligent manufacturing brought upon us.

References

[1] Raugei, M., *et al.*, The Energy Return on Energy Investment (EROI) of Photovoltaics: Methodology and Comparisons with Fossil Fuel Life Cycles, *Energy Policy*, *45* (2012), June, pp. 576-582

[2] Rekinger, M., *et al.*, Global Market Outlook for Solar Power/2015-2019, Report, Solar Industry Reports, Brussels, Belgium, 2015

[3] Medojevic, M., Medojevic, M., Simulation Based Productivity Forecast of 1 MW PV Power Plant in the Weather Conditions Typical for Belgrade Region, *International Journal of Industrial Engineering and Management (IJIEM)*, *8* (2017), 2, pp. 91-97

[4] Herrmann, C., *Ganzheitliches Life Cycle Management: Nachhaltigkeit und Lebenszyklusorientierung in Unternehmen* (in German), Springer-Verlag, Berlin Heidelberg, 2010, p. 423

[5] ***, United Nations, *Kyoto Protocol to the United Nations Framework Convention on Climate Change,* http://unfccc.int/resource/docs/convkp/kpeng.pdf (Accessed 10 March 2019)

[6] Duflou, J. R., *et al.*, Towards Energy and Resource Efficient Manufacturing: A Processes and Systems Approach, *CIRP Annals-Manufacturing Technology*, *61* (2012), 2, pp. 587-609

[7] Medojevic, M., *et al.*, Energy Management in Industry 4.0 Ecosystem: A Review on Possibilities and Concerns, *Proceedings*, 29th DAAAM International Symposium, B. Katalinic (Ed.), Published by DAAAM International, ISBN 978-3-902734-20-4, ISSN 1726-9679, Vienna, Austria, pp. 0674-0680

[8] Pavlović, T., *et al.*, Simulation of Photovoltaic Systems Electricity Generation Using HOMER Software in Specific Locations in Serbia, *Thermal Science*, *17* (2013), 2, pp. 333-347

[9] Klise, G. T., Stein, J. S., Models Used to Assess the Performance of Photovoltaic Systems, SANDIA REPORT, SAND2009-8258, 2009, Available online at: http://www.osti.gov/bridge

[10] Lalwani, M., *et al.*, Investigation of Solar Photovoltaic Simulation Softwares, *International Journal of Applied Engineering Research*, *1* (2010), 3, pp. 585-601

[11] ***, http://www.appropedia.org/Solar_photovoltaic_software

[12] Chandrakant, D., *et al.*, Performance Simulation of Grid-Connected Rooftop Solar PV System for Small Households: A Case Study of Ujjain, India, *Energy Reports*, *4* (2018), Nov., pp. 546-553

[13] Zeyringer M., *et al.*, Analyzing Grid Extension and Stand-Alone Photovoltaic Systems for the Cost-effective Electrification of Kenya, *Energy for Sustainable Development*, *25* (2015), Apr., pp. 75-86

[14] Shukla A. K., *et al.*, Exergetic Assessment of BIPV Module Using Parametric and Photonic Energy Methods: A Review, *Energy and Buildings*, *119* (2016), May, pp. 62-73

[15] Gilman, P., *et al.*, SAM Photovoltaic Model Technical Reference Update. Technical Report, 93 pp., (2018), NREL/TP-6A20-67399, Golden, Cal., USA

[16] Michalsky, J., The Astronomical Almanac's Algorithm for Approximate Solar Position (1950-2050), *Solar Energy*, *40* (1988), 3, pp. 227-235

[17] Iqbal, M., *An Introduction to Solar Radiation*, Academic Press, New York, USA, 1983

[18] O'Brien, J., Position of the Sun Given Time of Day, Latitude and Longitude, (2012), stack-overflow.com.http://stackoverflow.com/questions/8708048/position-of-the-sun-given-time-of-day-latitude-and-longitude

[19] Duffie, J., Beckman, W., *Solar Engineering of Thermal Processes*, 4th ed., Wiley, New York, USA, 2013

[20] Dunlap, J., *Photovoltaic Systems*, American Technical Publishers, Homewood, Ill., USA, 2007

[21] Freeman, J., *et al.*, Using Measured Plane-of-Array Data Directly in Photo-voltaic Modeling: Methodology and Validation, *Proceedings,* 43rd IEEE Photovoltaic Specialists Conference, Portland, Ore., USA, 2016, NREL/PO-6A20-66524.http://www.nrel.gov/docs/fy16osti/66524.pdf

[22] Dobos, A., PVWatts Version 1 Technical Reference, TP-6A20-60272, National Renewable Energy Laboratory, 2013, Golden, Cal., USA, http://www.nrel.gov/docs/fy14osti/60272.pdf

[23] Perez, R., *et al.*, The Development and Verification of the Perez Diffuse Radiation Model, SAN88-7030, Sandia National Laboratories, 1988, Albuquerque, N. Mex., USA, http://prod.sandia.gov/techlib/access-control.cgi/1988/887030.pdf

[24] Perez, R., *et al.*, Modeling Daylight Availability and Irradiance Components from Direct and Global Irradiance, *Solar Energy, 44*, (1990), 5, pp. 271-289

[25] ***, "Perez Sky Diffuse Model", Modeling Steps, PV Performance Modeling Collaborative, Sandia National Laboratories, 2014, Al-buquerque, N. Mex., USA, https://pvpmc.sandia.gov/modeling-steps/1-weather-design-inputs/plane-of-array-poa-irradiance/calculating-poa-irradiance/poa-sky-diffuse/perez-sky-diffuse-model/

[26] Liu, B., Jordan, R., A Rational Procedure for Predicting The Long-term Average Performance of Flat plate Solar energy Collectors, *Solar Energy, 7* (1963), 2, pp. 53-74

[27] Appelbaum, J., Bany, J., Shadow Effect of Adjacent Solar Collectors in Large Scale Systems, *Solar Energy*, *23* (1979), 6, pp. 497-507
[28] Deline, C., *et al.*, A Simplified Model of Uniform Shading in Large Photovoltaic Arrays, *Solar Energy*, *96* (2013), Oct., pp. 274-282
[29] De Soto, W., *et al.*, Improvement and Validation of a Model for Photovoltaic Array Performance, *Solar Energy*, *80* (2004), 1, pp. 78-88
[30] De Soto, W., *Improvement and Validation of a Model for Photovoltaic Array Performance,* University of Wisconsin-Madison, Madison, Wis., USA, 2004, http://sel.me.wisc.edu/publications/theses/desoto04.zip
[31] Marion, W., Measured and modeled photovoltaic system energy losses from snow for Colorado and Wisconsin locations, *Solar Energy*, *97* (2013), Nov., pp. 112-121
[32] Ryberg, D., Freeman, J., Integration, Validation and Application of a PV Snow Coverage Model in SAM, TP-6A20-64260, National Renewable Energy Laboratory, Golden, Cal., USA, 2015, http://www.nrel.gov/docs/fy15osti/64260.pdf
[33] King, D., *et al.*, Performance Model for Grid-Connected Photovoltaic Inverters, 47 pp.; Albuquerque, NM: Sandia National Laboratories, SAND2007-5036, (2007), http://prod.sandia.gov/techlib/access-control.cgi/2007/075036.pdf
[34] Ceylan, I., *et al.*, Cooling of a Photovoltaic Module with Temperature Controlled Solar Collector, *Energy and Buildings*, *72* (2014), Apr., pp. 96-101
[35] Moharram, K. A., *et al.*, Enhancing the Performance of Photovoltaic Panels by Water Cooling, *Ain Shams Engineering Journal*, *4* (2013), 4, pp. 869-877
[36] Bahaidarah, H., *et al.*, Performance Evaluation of a PV (Photovoltaic) Module by Back Surface Water Cooling for Hot Climatic Conditions, *Energy*, *59* (2013), Sept., pp. 445-453
[37] Alami, A. H., Effects of Evaporative Cooling on Efficiency of Photovoltaic Modules, *Energy Conversion and Management*, *77* (2014), Jan., pp. 668-679
[38] Irwan, Y. M., *et al.*, A New Technique of Photovoltaic/Wind Hybrid System in Perlis, *Energy Procedia*, *36* (2013), Dec., pp. 492-501
[39] Teo, H. G., *et al.*, An Active Cooling System for Photovoltaic Modules, *Applied Energy*, *90* (2012), 1, pp. 309-315
[40] Du, B., *et al.*, Performance Analysis of Water Cooled Concentrated Photovoltaic (CPV) System, *Renewable & Sustainable Energy Reviews*, *16* (2012), 9, pp. 6732-6736
[41] Dorobanțu, L., *et al.*, Experimental Assessment of PV Panels Front Water Cooling Strategy, *Proceedings*, International Conference on Renewable Energies and Power Quality (ICREPQ'13), Bilbao, Spain, 2013, pp. 1-4
[42] Rahimi, M., *et al.*, Design of a Self-Adjusted Jet Impingement System for Cooling of Photovoltaic Cells, *Energy Conversion and Management*, *83* (2014), July, pp. 48-57
[43] Al-shamani, A. N., *et al.*, Nanofluids for Improved Efficiency in Cooling Solar Collectors – A Review, *Renewable & Sustainable Energy Reviews*, *38* (2014), Oct., pp. 348-367
[44] ***, Aurora, The Ultimate Guide to PV System Losses – A Solar Designer's Guide for More Accurate Energy Production Estimates, 2018, pp. 22

Paper submitted: July 19, 2019
Paper revised: March 23, 2020
Paper accepted: March 28, 2020